Structure of a G protein-coupled receptor with GRK2 and a biased ligand

H. Eric Xu （✉ eric.xu@simm.ac.cn ）
 Shanghai Institute of Materia Medica (SIMM)   https://orcid.org/0000-0002-6829-8144

Jia Duan
 Shanghai Institute of Materia Medica (SIMM)

Heng Liu
 Shanghai Institute of Materia Medica (SIMM)

Yujie Ji
 Shanghai Institute of Materia Medica (SIMM)

Qingning Yuan
 Shanghai Institute of Materia Medica (SIMM)

Xinzhu Li
 Shanghai Institute of Materia Medica (SIMM)

Kai Wu
 Shanghai Institute of Materia Medica (SIMM)

Tianyu Gao
 Shanghai Institute of Materia Medica (SIMM)

Shengnan Zhu
 Macau University of Science and Technology

Yi Jiang
 Shanghai Institute of Materia Medica (SIMM)

Wanchao Yin
 Shanghai Institute of Materia Medica   https://orcid.org/0000-0002-6889-4907

Biological Sciences - Article

Keywords:

1 **Structure of a G protein-coupled receptor with GRK2 and a biased ligand**
2
3 Jia Duan[1, *, #], Heng Liu[1, *], Yujie Ji[1, 2, *], Qingning Yuan[1], Xinzhu Li[1, 3], Kai Wu[1], Tianyu
4 Gao[1, 4], Shengnan Zhu[5], Wanchao Yin[1], Yi Jiang[6], H. Eric Xu[1, 2, 4, #]
5
6 [1]State Key Laboratory of Drug Research, Shanghai Institute of Materia Medica,
7 Chinese Academy of Sciences, Shanghai 201203, China
8 [2]University of Chinese Academy of Sciences, Beijing 100049, China
9 [3]School of Chinese Materia Medica, Nanjing University of Chinese Medicine, Nanjing,
10 210023 China
11 [4]School of Life Science and Technology, ShanghaiTech University, Shanghai 201210,
12 China
13 [5]School of Pharmacy, Macau University of Science and Technology, Macau 999078,
14 China
15 [6]Lingang Laboratory, Shanghai 200031, China
16 *These authors contributed equally.
17 #**Co-corresponding authors:**
18 H.E.X., email: eric.xu@simm.ac.cn
19 J.D., email: duanjia@simm.ac.cn
20

Abstract

Phosphorylation of G protein-coupled receptors (GPCR) by GPCR kinases (GRKs) desensitizes G protein signaling and promotes arrestin signaling, which is also modulated by biased ligands[1-6]. Molecular assembly of GRKs to GPCRs and the basis of GRK-mediated biased signaling remain largely unknown due to the weak GPCR-GRK interactions. Here we report the complex structure of neurotensin receptor 1 (NTSR1) bound to GRK2, Gαq, and an arrestin-biased ligand, SBI-553[7], at a resolution of 2.92 Å. The high-quality density map reveals the clear arrangement of the intact GRK2 with the receptor, with the N-terminal helix of GRK2 docking into the open cytoplasmic pocket formed by the outward movement of the receptor TM6, analogous of the binding of G protein to the receptor. Strikingly, the arrestin-biased ligand is found at the interface between GRK2 and NTSR1 to enhance GRK2 binding. The binding mode of the biased ligand is compatible with arrestin binding but is clashed with the binding of a G protein, thus provide an unambiguous mechanism for its arrestin-biased signaling capability. Together, our structure provides a solid model for understanding the details of GPCR-GRK interactions and biased signaling.

GPCRs comprise the largest family of cell surface receptors whose signaling is primarily mediated by two types of downstream effectors: G-proteins and arrestins. The switch of GPCR signaling from G-protein pathways to arrestin pathways is controlled by a small family of GPCR kinases, GRKs, which phosphorylate either the receptor C-terminal tail or the third intracellular loop (ICL3)[1-3]. Phosphorylation of GPCRs promotes recruitment of arrestin, which blocks G-protein binding and desensitizes G-protein signaling[3]. Because drugs that selectively activate either G-protein pathways or arrestin pathways (biased signaling) are proposed to have better therapeutic and safety index[4,5], the mechanism of GPCR biased signaling has been a subject of intensive research over the past two decades.

50 GRK2, along with GRK1, are the prototypes of GRKs that belong to the AGC family of

51 serine/threonine kinases[8-10]. There are seven GRKs, which can be grouped into the

52 rhodopsin kinase subfamily (GRK1 and GRK7), the β-adrenergic receptor kinase

53 subfamily (GRK2 and GRK3), and the GRK4 subfamily (GRK4, GRK5 and GRK6)[9]. All

54 GRKs share conserved sequence features and structural arrangements[11]. At the N-

55 terminus is a conserved segment that formed a helix in the active GRK structures,

56 followed by the first eight helices of a regulatory G-protein signaling homology domain

57 (RHD)[10,12]. The kinase domain (KD) is inserted into a loop between helices 8 and 9 of

58 RHD, a conserved domain of a nine-helix bundle found in regulatory G-protein

59 signaling proteins[13]. Following the kinase domain and helix 9 of RHD are the less

60 conserved C-terminal GRK domains, which are mainly responsible for membrane

61 binding[14]. In the case of GRK2, its C-terminus contains a pleckstrin homology domain

62 (PHD) that interacts with Gβγ subunits of G protein[15]. The RHD of GRK2 also interacts

63 with Gαq when it is in complex with GTP[16]. The binding of both Gαq and Gβγ subunits

64 to GRK2 facilitates its membrane association[15,16].

65

66 As GPCR signal transducers like G proteins and arrestins, GRKs are rest at the basal

67 state, and can be recruited and activated by active GPCRs[3]. The molecular basis of

68 how GPCR signal transducers recognize and regulate GPCR signaling has been a

69 research focus of GPCR structural biology[14,17-21]. Structures of many GPCR-G protein

70 complexes and GPCR-arrestin complexes have been solved, which reveal that both G

71 proteins and arrestins recognize the open cytoplasmic pocket induced by the outward

72 movement of TM6 in the activated GPCRs[19,20,22-25]. Due to much weaker interactions

73 between GPCR and GRKs, high resolution structure of a GPCR-GRK complex is

74 technically challenging. A structure of rhodopsin in complex with GRK1 has provided a

75 breakthrough view of the overall assembly of GRK1 with rhodopsin via its N-terminal

76 helix[18]. However, the relatively low resolution of the structure lacks the density for the

77 conserved RHD domain of GRK1 and limits the detailed understanding of rhodopsin-

78 GRK1 interactions and GRK1 activation by the active rhodopsin.

79

Neurotensin receptor 1 (NTSR1) is a class A GPCR that is regulated by an endogenous peptide ligand, neurotensin (NTS)[26]. Up on activation, NTSR1 couples to various signal effectors, including several subtypes of G proteins, GRKs, and arrestins, to mediate neurotransmission and neuromodulation in the central nervous system[26-28]. Because of its diverse physiological roles, NTSR1 has been proposed as a drug target for addiction, obesity, analgesia, cancer, Parkinson's disease, and schizophrenia[7]. Structures of NTSR1 in complex with Gi or beta-arrestin have been determined by cryo-electron microscopy (cryo-EM)[22,23,29]. Notably, SBI-553, a β-arrestin-biased allosteric ligand of NTSR1 that antagonizes G-protein signaling, selectively reduces addictive behaviors without the unwanted side effects of hypotension, hypothermia, and motor impairment, which are typically associated with balanced agonism of NTSR1 induced by neurotensin[7]. However, the structural basis of β-arrestin-biased agonism of SBI-553 remains unknown. In this paper, we report the structure of NTSR1 bound to NTS, GRK2, Gαq, and SBI-553 at a resolution of 2.92 Å, which reveals detailed interactions between NTSR1 and GRK2, and provides a molecular explanation for the β-arrestin-biased agonism of SBI-553.

Complex assembly and structure determination

To identify a stable GPCR–GRK2 complex, we used Tango assays[30] to screen various members of class A GPCRs, and NTSR1 turned out to be one of the strongest receptors that interact with GRK2 (Extended Data Fig. 1a). Addition of SBI-553 further increased NTSR1-GRK2 interaction (Fig. 1a). The presence of SBI-553 enhanced potency and efficacy of NTS to promote GRK2 recruitment to NTSR1 (Fig. 1b). Co-expression of NTSR1 with GRK2 as well as Gαq and Gβγ formed a complex that could be purified to homogeneity but it was unstable (Extended Data Fig. 1b). We introduced the NanoBiT tethering strategy[31,32] to stabilize the complex by fusing LgBiT to the C-terminus of NTSR1 and HiBiT to the C-terminus of GRK2. The purification of the above complex showed a sub-stoichiometry ratio of the Gβγ subunit (Extended Data Fig. 1c),

108   indicating instable association of the Gβγ subunit with the rest of the complex. We thus

109   omitted the Gβγ subunit from the final complex assembly, which was further stabilized

110   by chemical crosslinking with BS$_3$ for cryo-EM studies (Extended Data Fig. 1d-f).

111

112   A total of 57,477 film images were collected, which yield ~40 million initial particles.

113   Further 2D and 3D classifications generate two maps at resolutions of 2.92 Å and 3.09

114   Å (Extended Data Fig. 2). The data and structure statistics are summarized in

115   Extended Data Table 1. Both maps were sufficiently clear to place NTSR1, NTS, GRK2,

116   Gαq, and the bound SBI-553, staurosporine, and GDP·AlF$_4^-$·Mg^{2+} (Fig. 1c, 1d and

117   Extended Data Fig. 2, 3). Comparison of these two complexes reveals that they have

118   very similar NTSR1 structure but a swing of GRK2 of ~5-6 Å related to NTSR1

119   (Extended Data Fig. 4), suggesting the dynamics of the NTSR1-GRK2 complex

120   assembly. 3D variability analysis (3DVA) of the two cryo-EM maps also reveal dynamic

121   swing of GRK2 around NTSR1, especially the Gαq subunit and the relative positions

122   between the RHD and kinase domain (Extended Data movie). Complex 1 (Figure 1c)

123   has higher resolution and is thus used for detailed analysis below.

124

125   **Structure of NTSR1-GRK2-SBI-553 complex**

126   Within the complex structure, NTSR1 resembles the NTSR1 structure in complex with

127   Gi and β-arrestin[22,23,29] (Fig. 2a), with an overall RMSD less than 1.0 Å for the entire

128   Cα atoms of NTSR1. Compared to the inactive NTSR1 structure, conformational

129   changes mainly occurred at cytoplasmic ends of TM5 (4.5 Å shift), TM6 (11.3 Å shift)

130   and TM7 (1.7 Å shift), consistent with an active conformation of NTSR1 (Fig. 2a).

131

132   At the extracellular side, NTS, the peptide ligand, is fit into the top-central TMD pocket

133   (Fig. 2b). At the intracellular side, SBI-553 is found at the bottom-central cytoplasmic

134   pocket, Underneath SBI-553 is the N-terminal helix of GRK2, which docks into the

135   open cytoplasmic pocket. The overall structure of NTSR1-GRK2 complex is similar to

136   the rhodopsin-GRK1 complex[18] (Fig. 2c), however, the position of the N-terminal helix

137　of GRK2 is shift by as much as 8.0 Å relative to the N-terminal helix of GRK1 (Fig. 2c).

138　Correspondingly, the whole kinase domain of GRK2 is shift by as much as 7-8 Å from

139　the GRK1 kinase domain (Fig. 2c).

140

141　Compared to the partial GRK1 structure in the rhodopsin-GRK1 complex, GRK2 from

142　the NTSR1-GRK2 complex has nearly complete structure with RH and PH domains

143　clearly defined in the structure (Fig. 2c). In the structure, Gαq is bound to the RHD of

144　GRK2 (Fig. 2d). Comparing the GRK2 structure from the NTSR1 complex to the crystal

145　structure of GRK2 from the complex with Gαq and Gβγ reveals three major differences

146　as below[16] (Extended Data Fig. 5). The GRK2 structure from the NTSR1 complex

147　contains a N-terminal helix that is packed onto the kinase domain (Extended Data Fig.

148　5), has a breakage in the ionic lock between its RHD from the KD, and adopts a closed

149　conformation in its kinase domain that is in the active state (Extended Data Fig. 5). In

150　contrast, the GRK2 crystal structure from the complex with Gαq and Gβγ does not

151　have the N-terminal helix, contains the ionic lock between its RHD and the KD as seen

152　in the GRK5 structure[14,33], and adopts an open conformation in its kinase domain,

153　resembling the inactive state (Extended Data Fig. 5).

154

155　The overall arrangement of the NTSR1-GRK2 complex also present possible

156　association of GRK2 with the membrane lipid layer (Fig. 2d). Alignment of H8 of NTSR1

157　with the membrane layer reveals that the C-terminal tip of helix 9 from RHD, the loop

158　between β-strands 1 and 2, and the loop between β-strands 5 and 6 from PHD are in

159　close contact with the membrane layer (Fig. 2d, Extended Data Fig. 6). Additional

160　binding of GRK2 to the membrane layer could come from lipid modifications in the Gα

161　and Gγ subunits (Fig. 2d). Modeling of the Gβγ subunit into the NTSR1-GRK2 structure

162　suggest that the C-terminal lipid modification of the Gγ subunit is also close to the

163　membrane layer (Fig. 2d). In addition, superposition of GRK5 to GRK2 in the NTSR1-

164　GRK2 complex reveals that the N-terminal lipid binding domain (NLBD) and C-terminal

165　lipid binding domain (CLBD) of GRK5 are near the membrane layer (Fig. 2d, Extended

Data Fig. 6), consistent with their roles in lipid binding[14].

167

168 **The GRK2-NTSR1 interface**

169 The GRK2-NTSR1 interface is at the center of the complex, which has relatively high

170 resolution at ~2.5 Å (Extended Data Fig. 2c, 2d), thus the density map is clear for

171 interface residues, which reveals detailed intermolecular interactions between GRK2

172 and NTSR1 at the residue-specific levels (Fig. 3). The GRK2-NTSR1 complex has

173 one major interface comprised by the N-terminal helix of GRK2, which inserts into the

174 open TM6 pocket (Fig. 3a, 3b), and one minor interface comprised by ICL2 of NTSR1

175 that interact with the loop between the N-terminal helix and the RHD (Fig. 3c).

176

177 At the major interface, five hydrophobic residues (L4, V7, L8, V11, and M15) from the

178 N-terminal helix of GRK2 form an extended hydrophobic patch, which is packed

179 against a hydrophobic pocket formed by hydrophobic residues from TM5, TM6, and

180 TM7 (L263$^{5.65}$, M266$^{5.68}$, A297$^{6.29}$, L298$^{6.30}$, G301$^{6.33}$, and V367$^{7.56}$) (Fig. 3a). In addition,

181 the carboxylate side chain of D3 forms a network of hydrogen bonds with the main

182 chain amine groups of A369$^{8.48}$ and N370$^{8.49}$, and the side chains of S368$^{8.47}$ and

183 N370$^{8.49}$. R294$^{6.26}$ also forms a direct hydrogen bond with the main chain carbonyl from

184 G475 of GRK2 (Fig. 3b). These additional hydrogen bonds may also help to stabilize

185 the N-terminal helix of GRK2 in the cytoplasmic pocket. At the ICL2 minor interface,

186 F174 is packed against the main chain of N189 from GRK2, K177 forms a hydrogen

187 bond with the main chain carbonyl of F191 from the GRK2 kinase domain, and T178

188 forms a hydrogen bond with the side chain of N189 (Fig. 3c). The total buried surface

189 area between GRK2 and NTSR1 is 746 Å^2, which is considerably smaller than the

190 NTSR1-Gi interface of 1197 Å^2, consistent with the relatively weak NTSR1-GRK2

191 interactions.

192

193 **The basis of SBI-553 biased agonism**

194 SBI-553 is an arrestin-biased PAM ligand that specifically blocks G protein signaling

195   but enhances arrestin signaling[7]. The high-quality density map clearly defines the

196   binding mode of SBI-553 (Fig. 4), which adopts an inverted T-shape configuration and

197   binds to the interface between NTSR1 and GRK2 (Fig. 4a, 4b). In the structure, SBI-

198   553 forms extensive interactions with both receptor and GRK2 as summarized in

199   Extended Data Table 2. Specifically, with the receptor, SBI-553 form predominately

200   hydrophobic interactions with residues from TM2, TM3, TM5, TM6, TM7, and H8 (Fig.

201   4c, 4d). With GRK2, SBI-553 forms direct interactions with L4, E5, and L8 from the N-

202   terminal helix (Fig. 4d), consistent with the enhanced binding of GRK2 to NTSR1 by

203   SBI-553 (Fig. 1a, 1b).

204

205   The binding site of SBI-553 is unique and unexpected, which has not been observed

206   in any GPCR structures determined to date[34,35]. Structure superposition of NTSR1 from

207   its Gi complex onto the NTSR1-GRK2 structure reveal that the α5 helix from the G

208   proteins occupies roughly the same space as occupied by the N-terminal helix of GRK2

209   (Extended Data Fig. 7). However, the α5 helix from the Gαi is up-shift by as much as

210   8.0 Å into the TMD pocket related to the N-terminal helix of GRK2 (Extended Data Fig.

211   7). In this orientation, the α5 helix from the Gαi would clash directly with the bound SBI-

212   553 (Fig. 4e), thus providing a direct explanation for inhibition of G protein signaling by

213   SBI-553. Importantly, structural superposition of NTSR1 from its arrestin complex

214   reveals that the binding of SBI-553 would be compatible with arrestin binding to NTSR1

215   (Fig. 4f), consistent with its arrestin-biased signaling property.

216

217   **Universal features of GPCR-GRK interactions**

218   In this paper, we have determined the structure of NTSR1 in complex with GRK2 and

219   SBI-553 at a resolution of 2.92 Å, with the interface region approaching to 2.5 Å

220   (Extended Data Fig. 2c, 2d). The relatively high resolution of the structure provides a

221   clear binding mode of GRK2 and SBI-553 to NTSR1 as well as the mode of GRK2

222   membrane association. The primary binding site of GRK2 at NTSR1 is overlapped with

223   the NTSR1 Gi binding site comprised by TM6, TM7 and H8, which structural features

224   are highly similar in the active structures of various GPCRs (Extended Data Fig. 8),

225   thus providing a basis for GRK2's capability to interact with many different GPCRs.

226

227   In addition, the binding site of GRK2 at NTSR1 is the same as the GRK1 binding site

228   in rhodopsin (Fig. 2c). In our structure, GRK2 has nearly complete structure with clear

229   definition of many flexible regions, including the RHD and the active site tether (AST)

230   loop, which tether the kinase domain in the active conformation. The residues from the

231   N-terminal helix of GRK2 that interact with NTSR1 are highly conserved in all GRKs,

232   suggesting the binding mode of GRK2 is a universal feature for all GRKs (Extended

233   Data Fig. 6).

234

235   Finally, our structure reveals an unexpected binding mode of SBI-553, which is docked

236   at the interface between GRK2 and NTSR1, consistent with its ability to enhance GRK2

237   binding to NTSR1 (Fig. 1a, 1b, 2b). The binding of SBI-553 is compatible with arrestin

238   binding but would clash with G proteins (Fig. 4e, 4f), thus providing a direct mechanism

239   for its arrestin-biased signaling capability. Together, our structure provides a solid

240   model (Fig. 5) for understanding the details of GPCR-GRK interactions and biased

241   signaling, and a basis for designing arrestin-biased ligands for NTSR1 and possibly

242   other GPCRs.

243

244

Method

Constructs

Human NTSR1 (residues 1-418) was codon-optimized for Sf9 expression and cloned into a modified pFastBac vector, which contains an N-terminal hemagglutinin (HA) signal peptide followed by a flag tag and a b562RIL (BRIL) epitope before the receptor. To improve the complex homogeneity and stability, the NanoBiT tethering strategy was applied by fusing a LgBiT subunit (Promega) at the receptor C-terminus after a GSSGGSGGGG linker[31,32]. Bovine GRK2 was cloned with a C-terminal GSSGGSGGGG linker followed by the HiBiT (peptide86) subunit[32]. Additionally, three mutations (A292P, R295I and S455D) were also incorporated into GRK2 by site-directed mutagenesis to enhance the affinity between GRK2 and Fab6[18]. Gαq construct was modified into a pFastBac vector. And the native N terminus (residues 1-28) of Gαq was replaced with Gαi1 to facilitate the expression of Gαq[16].

Expression and purification of NTSR1-GRK2-Gαq complex

NTSR1-LgBiT, Gαq, GRK2-HiBiT and Ric8a (a gift from Brian Kobilka) were co-expressed in *Sf9* insect cells (Invitrogen) using the Bac-to-Bac baculovirus expression system (ThermoFisher). Cell pellets were thawed and lysed in 20 mM HEPEs, pH 7.4, 100 mM NaCl, 10% glycerol, 10 mM $MgCl_2$, 10 mM NaF and 30 µM $AlCl_3$ supplemented with Protease Inhibitor Cocktail, EDTA-Free (TargetMol). The NTSR1-GRK2-Gαq complex was formed in membranes by the addition of 10 µM NTS (Genscript), 10 µM saturosporine, 10 µM SBI-553 (TargetMol) and 50 µM GDP. The suspension was incubated for 0.5 h at room temperature before centrifugation at 80,000 × g for 30 min. The membrane was then resuspended with the same buffer and solubilized using 0.5% (w/v) n-dodecyl β-D-maltoside (DDM, Anatrace), 0.1% (w/v) cholesterol hemisuccinate (CHS, Anatrace) for 2 h at 4 °C. The supernatant was collected by centrifugation at 80,000 × g for 40 min and then incubated with G1 anti-Flag affinity resin (Genscript) for 2 h at 4 °C. After batch binding, the resin was loaded into a plastic gravity flow column and washed with 20 column volumes of 20 mM HEPEs, pH 7.4, 100 mM NaCl,

274 10% glycerol, 10 mM $MgCl_2$, 10 mM NaF, 30 µM $AlCl_3$, 10 µM NTS, 10 µM

275 saturosporine, 10 µM SBI-553 and 50 µM GDP, 0.01% (w/v) DDM, 0.002%(w/v) CHS,

276 and 0.05%(w/v) digitonin, further eluted with 10 column volumes of the same buffer

277 plus 0.2 mg/mL Flag peptide. The complex was then concentrated using an Amicon

278 Ultra Centrifugal Filter (MWCO 100 kDa) and injected onto a Superose 6 Increase

279 10/300 GL column (GE Healthcare) equilibrated in the buffer containing 20 mM HEPEs,

280 pH 7.4, 100 mM NaCl, 10 mM $MgCl_2$, 10 mM NaF, 30 µM $AlCl_3$, 10 µM NTS, 10 µM

281 saturosporine, 5 µM SBI-553, 50 µM GDP, and 0.03% (w/v) digitonin. To stabilize the

282 NTSR1-GRK2-Gαq complex, the peak fractions were collected and crosslinked using

283 0.01 mM BS_3 for 0.5 h at room temperature, stopped crosslinking by addition of 80 mM

284 of glycine, and then concentrated to approximately 10 mg/ml for cryo EM analysis.

285

286 **Cryo-EM grid preparation and data collection**

287 For the preparation of cryo-EM grids, 3 µL of the purified protein at 10 mg/mL were

288 applied onto a glow-discharged holey carbon grid (CryoMatrix Amorphous alloy film

289 R1.2/1.3, 300 mesh). Grids were plunge-frozen in liquid ethane using Vitrobot Mark IV

290 (Thermo Fischer Scientific). Frozen grids were transferred to liquid nitrogen and stored

291 for data acquisition. Cryo-EM imaging of the complex was performed on a Titan Krios

292 at 300 kV in the Advanced Center for Electron Microscopy at Shanghai Institute of

293 Materia Medica, Chinese Academy of Sciences (Shanghai China).

294

295 A total of 57,477 movies for the NTSR1-GRK2-Gαq complex were collected by a Gatan

296 K3 Summit direct electron detector with a Gatan energy filter (operated with a slit width

297 of 20 eV) (GIF) at a pixel size of 0.824 Å using the EPU software. The micrographs

298 were recorded in counting mode with a defocus ranging from -1.2 to -2.2 µm. The total

299 exposure time was 3.33 s with a dose of 50 electrons, and intermediate frames were

300 recorded in 0.104 s intervals, resulting in a total of 36 frames per micrograph.

301

302 **Image processing and map construction**

303   A total of 57,477 dose-fractioned movies were used for correction of beam-induced

304   movement using a dose-weighting scheme in MotionCor2[36] and their contrast transfer

305   function parameters were estimated by Patch CTF estimation in CryoSPARC[37]. For

306   the NTSR1-GRK2-Gαq complex, particle selection was performed by blob picking

307   using CryoSPARC[37], and 40,940,867 particles were extracted and further subjected to

308   an initial reference-free 2D classification. Interactive 2D and 3D classifications were

309   performed to discard poorly defined particles, and 1,149,932 particles were retained.

310   These particles were divided into 6 subclasses using Ab-initial model and hetero-

311   refinement, resulting in two subsets with complete NTSR1-GRK2-Gαq complex. Two

312   maps from the two subsets showed slightly difference especially relative position of

313   GRK2 and Gαq. We merged the two subsets, and performed another round of Ab-

314   initial model and hetero-refinement to remove particles without clear NTSR1-GRK2-

315   Gαq complex. In the 5 subclasses, two well-defined subsets, containing 287,853

316   particles and 216,282 particles, respectively, were subsequently subjected to non-

317   uniform refinement in CryoSPARC[37], generated two different maps with global

318   resolution of 2.92 Å and 3.09 Å. Resolution was estimated in the presence of a soft

319   solvent mask and based on the gold standard Fourier shell correlation (FSC) 0.143

320   criterion. Local resolution was estimated in cryoSPARC[37] using default parameters.

321   Unless indicated otherwise, the maps shown in figures were sharpened with B factors

322   estimated in the nonuniform refinement.

323

324   To analyze the flexibility of the NTSR1-GRK2-Gαq complex, we performed cryoSPARC

325   3D variability analysis (3DVA)[38]. The 3DVA was performed with mask on the complex,

326   generated from non-uniform refinement. The 3DVA was analyzed across three

327   principal components that estimated the most common motions. One of the

328   components showed pronounced motion between GRK2 and Gαq and the movie that

329   consisted of 20 volume frame data were presented by Chimera (v1.4) in the Extended

330   Data movie.

331

Model building and refinement

For the NTSR1-GRK2-Gαq complexes, the AlphaFold model of NTSR1 and the structure of G Protein-Coupled Receptor Kinase 2 in Complex with Gαq and Gβγ Subunits (PDB code: 2BCJ), were used as the start for model rebuilding and refinement against the electron microscopy map. The model was docked into the EM density map using Chimera[39], followed by iterative manual adjustment and rebuilding in COOT[40] and ISOLDE[41]. Real space and reciprocal space refinements were performed using Phenix[42] programs with secondary structure and geometry restraints. The final refinement statistics were validated using the module "comprehensive validation (cryo-EM)" in Phenix[42]. The final refinement statistics are provided in Extended Data Table 1. Structure figures were prepared in ChimeraX[43] and PyMOL (https://pymol.org/2/).

Calculation of NTSR1-Gi protein and NTSR1-GRK2 interface area

NTSR1-GRK2-Gαq complex and NTSR1-Gi protein complex (PDB ID: 6OS9) were used for the calculation of NTSR1-GRK2, NTSR1-Gi interface areas respectively, using PDBePISA web server (PDBe < PISA < EMBL-EBI). During the process, NTSR1-GRK2-Gαq complex and NTSR1-G protein complex were uploaded, and the Accessible surface area (ASA) calculations are based on finite element analysis through the "interface" module.

NanoBiT assay for GRK2 recruitment

The full-length NTSR1 (1–418) was cloned into pBiT1.1 vector (Invitrogen) with a FLAG tag at its N-terminus and LgBiT at its C-terminus. Bovine GRK2 (residues 1-689) was cloned into pBiT2.1 vector (Invitrogen) with a modified SmBiT (peptide104: MVEGYRLFEKIS)[31] and a GSSGGGGSGGGGSSG linker at its N-terminus. AD293 cells were cultured in DMEM/high Glucose (GE healthcare) supplemented with 10% (w/v) FBS (Gemini). Cells were maintained at 37 °C in a 5% CO2 incubator with 300,000 cells per well in a 6-well plate. Cells were grown overnight and then

361 transfected with 1.5 μg NTSR1 and 1.5 μg GRK2 constructs by FuGENE® HD

362 transfection reagent in each well for 24 h. Cells were harvested and re-suspended in

363 Hanks' balanced salt solution buffer (HBSS) at a density of 5×10^5 cells/ml. The cell

364 suspension was seeded in a 384-well plate at a volume of 10 μl per well, followed by

365 10 μl HBSS or 10 μl HBSS containing 1 μM SBI-553, 10 μl HBSS containing different

366 concentrations of NTS, and another 10 μl the NanoLuc substrate (furimazine, 1:25

367 dilution, Promega) diluted in the detection buffer. The luminescence signal was

368 measured with an EnVision plate reader at room temperature.

369

370 **Tango assay**

371 Human NTSR1 (1-418) was cloned into pcDNA6 vector consisting of an expression

372 cassette with tobacco etch virus (TEV) protease cleavage site and the transcriptional

373 activator tTA at the C terminus. A TEV protease cDNA was fused to the C-terminus of

374 GRK2 (1-689). Interaction between NTSR1 and GRK2 leads to the cleavage of the

375 TEV site, thus releasing tTA to trigger tTA-dependent luciferase reporter gene

376 expression. For Tango assays, HTL cells were cultured in 24-well plate at a density of

377 5×10^4 cells/well for 24 h, and then transfected with 10 ng NTSR1, 10 ng GRK2

378 plasmids and 5 ng of phRG-tk Renilla luciferase expression plasmids using FuGENE®

379 HD transfection reagent. After transfection for 24 h, cells were incubated overnight with

380 PBS (vehicle), or different concentrations of ligands. Then luciferase activities were

381 evaluated according to manufacturer's protocols of the Dual Luciferase Kit (Promega).

382

14

394   **Author contributions:**

References

1   Pitcher, J. A., Freedman, N. J. & Lefkowitz, R. J. G protein-coupled receptor kinases. *Annu Rev Biochem* **67**, 653-692, doi:10.1146/annurev.biochem.67.1.653 (1998).

2   Gurevich, E. V., Tesmer, J. J., Mushegian, A. & Gurevich, V. V. G protein-coupled receptor kinases: more than just kinases and not only for GPCRs. *Pharmacol Ther* **133**, 40-69, doi:10.1016/j.pharmthera.2011.08.001 (2012).

3   Gurevich, V. V. & Gurevich, E. V. GPCR Signaling Regulation: The Role of GRKs and Arrestins. *Front Pharmacol* **10**, 125, doi:10.3389/fphar.2019.00125 (2019).

4   Hodavance, S. Y., Gareri, C., Torok, R. D. & Rockman, H. A. G Protein-coupled Receptor Biased Agonism. *J Cardiovasc Pharmacol* **67**, 193-202, doi:10.1097/FJC.0000000000000356 (2016).

5   Rankovic, Z., Brust, T. F. & Bohn, L. M. Biased agonism: An emerging paradigm in GPCR drug discovery. *Bioorg Med Chem Lett* **26**, 241-250, doi:10.1016/j.bmcl.2015.12.024 (2016).

6   Seyedabadi, M., Gharghabi, M., Gurevich, E. V. & Gurevich, V. V. Structural basis of GPCR coupling to distinct signal transducers: implications for biased signaling. *Trends Biochem Sci* **47**, 570-581, doi:10.1016/j.tibs.2022.03.009 (2022).

7   Slosky, L. M. *et al.* beta-Arrestin-Biased Allosteric Modulator of NTSR1 Selectively Attenuates Addictive Behaviors. *Cell* **181**, 1364-1379 e1314, doi:10.1016/j.cell.2020.04.053 (2020).

8   Benovic, J. L., DeBlasi, A., Stone, W. C., Caron, M. G. & Lefkowitz, R. J. Beta-adrenergic receptor kinase: primary structure delineates a multigene family. *Science* **246**, 235-240, doi:10.1126/science.2552582 (1989).

9   Mushegian, A., Gurevich, V. V. & Gurevich, E. V. The origin and evolution of G protein-coupled receptor kinases. *PLoS One* **7**, e33806, doi:10.1371/journal.pone.0033806 (2012).

10   Sulon, S. M. & Benovic, J. L. Targeting G protein-coupled receptor kinases (GRKs) to G protein-coupled receptors. *Curr Opin Endocr Metab Res* **16**, 56-65, doi:10.1016/j.coemr.2020.09.002 (2021).

11   Ribas, C. *et al.* The G protein-coupled receptor kinase (GRK) interactome: role of GRKs in GPCR regulation and signaling. *Biochim Biophys Acta* **1768**, 913-922, doi:10.1016/j.bbamem.2006.09.019 (2007).

12   Beautrait, A. *et al.* Mapping the putative G protein-coupled receptor (GPCR) docking site on GPCR kinase 2: insights from intact cell phosphorylation and recruitment assays. *J Biol Chem* **289**, 25262-25275, doi:10.1074/jbc.M114.593178 (2014).

13   Baameur, F. *et al.* Role for the regulator of G-protein signaling homology domain of G protein-coupled receptor kinases 5 and 6 in beta 2-adrenergic receptor and rhodopsin phosphorylation. *Mol Pharmacol* **77**, 405-415, doi:10.1124/mol.109.058115 (2010).

14   Komolov, K. E. *et al.* Structural and Functional Analysis of a beta2-Adrenergic Receptor Complex with GRK5. *Cell* **169**, 407-421 e416, doi:10.1016/j.cell.2017.03.047 (2017).

15   Lodowski, D. T., Pitcher, J. A., Capel, W. D., Lefkowitz, R. J. & Tesmer, J. J. Keeping G proteins at bay: a complex between G protein-coupled receptor kinase 2 and Gbetagamma. *Science* **300**, 1256-1262, doi:10.1126/science.1082348 (2003).

16   Tesmer, V. M., Kawano, T., Shankaranarayanan, A., Kozasa, T. & Tesmer, J. J. Snapshot of activated G proteins at the membrane: the Galphaq-GRK2-Gbetagamma complex.

447   *Science* **310**, 1686-1690, doi:10.1126/science.1118890 (2005).

448   17   He, Y. *et al.* Molecular assembly of rhodopsin with G protein-coupled receptor kinases.
449   *Cell Res* **27**, 728-747, doi:10.1038/cr.2017.72 (2017).

450   18   Chen, Q. *et al.* Structures of rhodopsin in complex with G-protein-coupled receptor kinase
451   1. *Nature* **595**, 600-605, doi:10.1038/s41586-021-03721-x (2021).

452   19   Rasmussen, S. G. *et al.* Crystal structure of the beta2 adrenergic receptor-Gs protein
453   complex. *Nature* **477**, 549-555, doi:10.1038/nature10361 (2011).

454   20   Kang, Y. *et al.* Crystal structure of rhodopsin bound to arrestin by femtosecond X-ray laser.
455   *Nature* **523**, 561-567, doi:10.1038/nature14656 (2015).

456   21   Zhou, X. E. *et al.* Identification of Phosphorylation Codes for Arrestin Recruitment by G
457   Protein-Coupled Receptors. *Cell* **170**, 457-469 e413, doi:10.1016/j.cell.2017.07.002 (2017).

458   22   Yin, W. *et al.* A complex structure of arrestin-2 bound to a G protein-coupled receptor.
459   *Cell Res* **29**, 971-983, doi:10.1038/s41422-019-0256-2 (2019).

460   23   Huang, W. *et al.* Structure of the neurotensin receptor 1 in complex with beta-arrestin 1.
461   *Nature* **579**, 303-308, doi:10.1038/s41586-020-1953-1 (2020).

462   24   Staus, D. P. *et al.* Structure of the M2 muscarinic receptor-beta-arrestin complex in a lipid
463   nanodisc. *Nature* **579**, 297-302, doi:10.1038/s41586-020-1954-0 (2020).

464   25   Lee, Y. *et al.* Molecular basis of beta-arrestin coupling to formoterol-bound beta1-
465   adrenoceptor. *Nature* **583**, 862-866, doi:10.1038/s41586-020-2419-1 (2020).

466   26   Besserer-Offroy, E. *et al.* The signaling signature of the neurotensin type 1 receptor with
467   endogenous ligands. *Eur J Pharmacol* **805**, 1-13, doi:10.1016/j.ejphar.2017.03.046 (2017).

468   27   Rostene, W. H. & Alexander, M. J. Neurotensin and neuroendocrine regulation. *Front
469   Neuroendocrinol* **18**, 115-173, doi:10.1006/frne.1996.0146 (1997).

470   28   Inagaki, S. *et al.* G Protein-Coupled Receptor Kinase 2 (GRK2) and 5 (GRK5) Exhibit
471   Selective Phosphorylation of the Neurotensin Receptor in Vitro. *Biochemistry* **54**, 4320-
472   4329, doi:10.1021/acs.biochem.5b00285 (2015).

473   29   Kato, H. E. *et al.* Conformational transitions of a neurotensin receptor 1-Gi1 complex.
474   *Nature* **572**, 80-85, doi:10.1038/s41586-019-1337-6 (2019).

475   30   Barnea, G. *et al.* The genetic design of signaling cascades to record receptor activation.
476   *Proc Natl Acad Sci U S A* **105**, 64-69, doi:10.1073/pnas.0710487105 (2008).

477   31   Dixon, A. S. *et al.* NanoLuc Complementation Reporter Optimized for Accurate
478   Measurement of Protein Interactions in Cells. *ACS Chem Biol* **11**, 400-408,
479   doi:10.1021/acschembio.5b00753 (2016).

480   32   Duan, J. *et al.* Cryo-EM structure of an activated VIP1 receptor-G protein complex
481   revealed by a NanoBiT tethering strategy. *Nat Commun* **11**, 4121, doi:10.1038/s41467-
482   020-17933-8 (2020).

483   33   Komolov, K. E., Bhardwaj, A. & Benovic, J. L. Atomic Structure of GRK5 Reveals Distinct
484   Structural Features Novel for G Protein-coupled Receptor Kinases. *J Biol Chem* **290**,
485   20629-20647, doi:10.1074/jbc.M115.647297 (2015).

486   34   Draper-Joyce, C. J. *et al.* Positive allosteric mechanisms of adenosine A1 receptor-
487   mediated analgesia. *Nature* **597**, 571-576, doi:10.1038/s41586-021-03897-2 (2021).

488   35   Egyed, A., Kiss, D. J. & Keseru, G. M. The Impact of the Secondary Binding Pocket on the
489   Pharmacology of Class A GPCRs. *Front Pharmacol* **13**, 847788,
490   doi:10.3389/fphar.2022.847788 (2022).

491   36   Zheng, S. Q. *et al.* MotionCor2: anisotropic correction of beam-induced motion for
492   improved cryo-electron microscopy. *Nat Methods* **14**, 331-332, doi:10.1038/nmeth.4193
493   (2017).
494   37   Punjani, A., Rubinstein, J. L., Fleet, D. J. & Brubaker, M. A. cryoSPARC: algorithms for rapid
495   unsupervised cryo-EM structure determination. *Nat Methods* **14**, 290-296,
496   doi:10.1038/nmeth.4169 (2017).
497   38   Punjani, A. & Fleet, D. J. 3D variability analysis: Resolving continuous flexibility and discrete
498   heterogeneity from single particle cryo-EM. *J Struct Biol* **213**, 107702,
499   doi:10.1016/j.jsb.2021.107702 (2021).
500   39   Pettersen, E. F. *et al.* UCSF Chimera--a visualization system for exploratory research and
501   analysis. *J Comput Chem* **25**, 1605-1612, doi:10.1002/jcc.20084 (2004).
502   40   Emsley, P. & Cowtan, K. Coot: model-building tools for molecular graphics. *Acta
503   Crystallogr D Biol Crystallogr* **60**, 2126-2132, doi:10.1107/S0907444904019158 (2004).
504   41   Croll, T. I. ISOLDE: a physically realistic environment for model building into low-resolution
505   electron-density maps. *Acta Crystallogr D Struct Biol* **74**, 519-530,
506   doi:10.1107/S2059798318002425 (2018).
507   42   Adams, P. D. *et al.* PHENIX: a comprehensive Python-based system for macromolecular
508   structure solution. *Acta Crystallogr D Biol Crystallogr* **66**, 213-221,
509   doi:10.1107/S0907444909052925 (2010).
510   43   Pettersen, E. F. *et al.* UCSF ChimeraX: Structure visualization for researchers, educators,
511   and developers. *Protein Sci*, doi:10.1002/pro.3943 (2020).
512

Figure 1
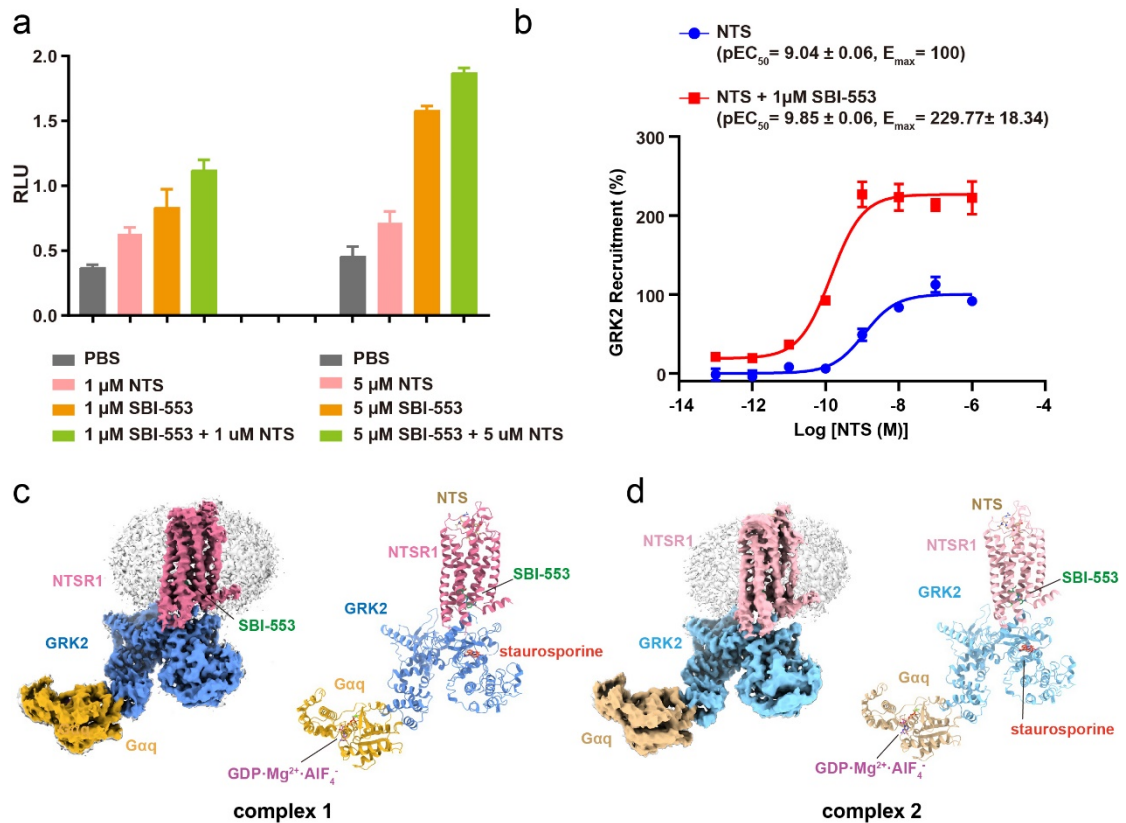
Fig. 1: Cryo-EM structures of the NTSR1-GRK2-Gαq complexes. a, NTS and SBI-553 improve NTSR1-GRK2 interaction determined by Tango assay. RLU, relative luciferase units. **b,** NTSR1-GRK2 recruitment promoted by addition of NTS and SBI-553 determined by NanoBiT assay. Data were shown as mean ± S.E.M. from three independent experiments (n=3), performed in triplicates. The representative concentration-response curves were shown. **c, d,** Cryo-EM density maps and ribbon presentation of the NTSR1-GRK2-Gαq complexes. Complex 1 (**c**) and complex 2 (**d**).

Figure 2
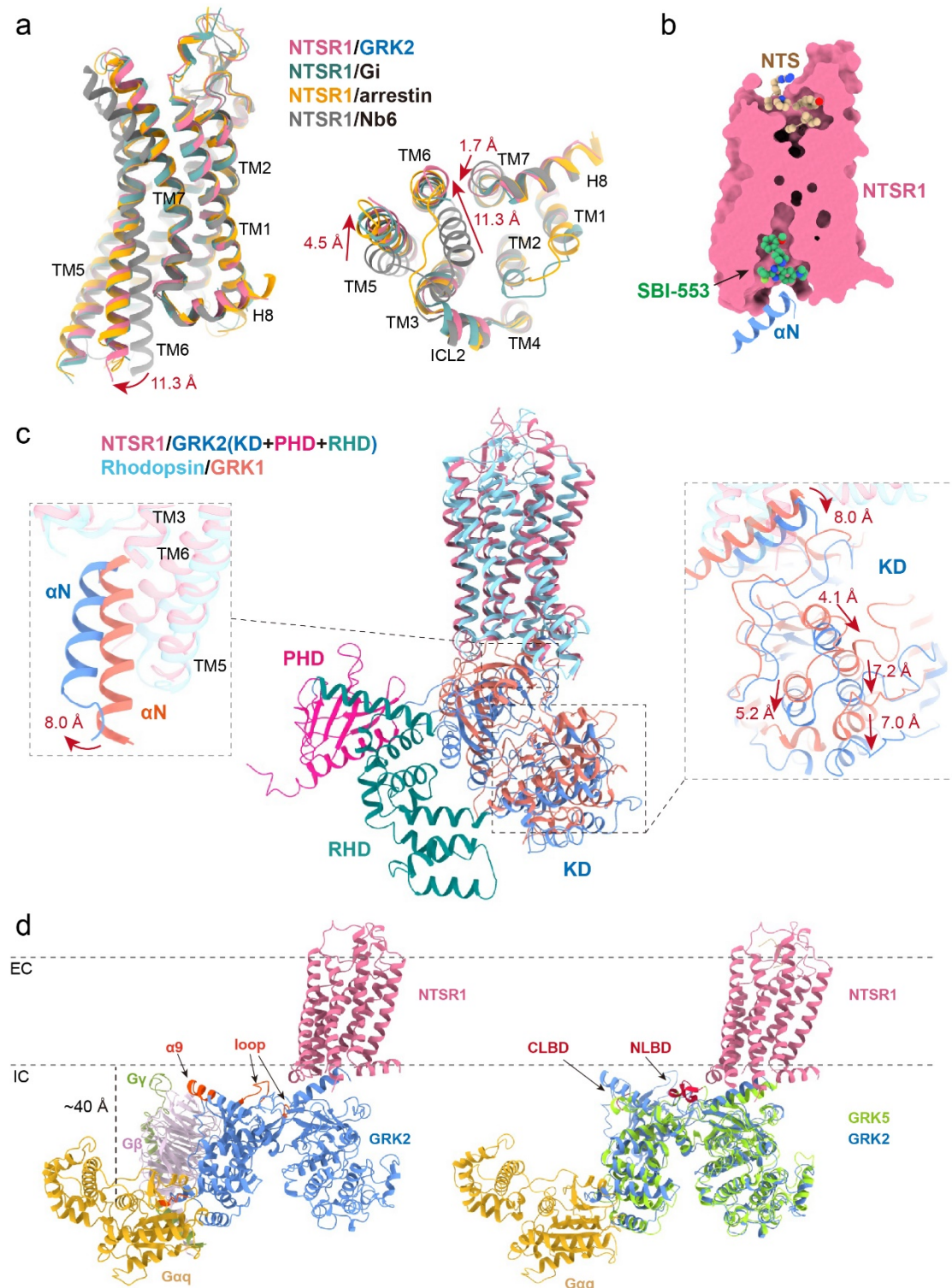
Fig. 2: Structural features of the NTSR1-GRK2-Gαq complex. a, Structural comparison of the NTSR1 from NTSR1-GRK2-Gαq complex with the inactive NTSR1 (PDB code: 7UL2), NTSR1 from NTSR1-arrestin2 complex (PDB code: 6UP7) and NTSR1 from NTSR1-Gi complex (PDB code: 6OS9). **b**, The overall arrangement of the NTS and SBI-

553 binding pockets in NTSR1. **c**, Structural comparison of the NTSR1-GRK2-Gαq complex with the rhodopsin-GRK1 complex (PDB code: 7MTA). KD, kinase domain. PHD, pleckstrin homology domain. RHD, regulatory G-protein signaling homology domain. **d,** Possible membrane binding sites of GRK2 and GRK5. The possible lipid binding sites from GRK2 are highlighted in orange, and the N-terminal lipid binding site (NLBD), the C-terminal lipid binding site (CLBD) of GRK5 (PDB code: 6PJX) are shown in dark red. α9, helix 9. EC, extracellular membrane layer. IC, intracellular membrane layer. The distance between the N-terminal of Gαq with the intracellular membrane layer is around 40 Å, which could be reached by the stretch loop of 38 residues from the N-terminus of Gαq.

Figure 3
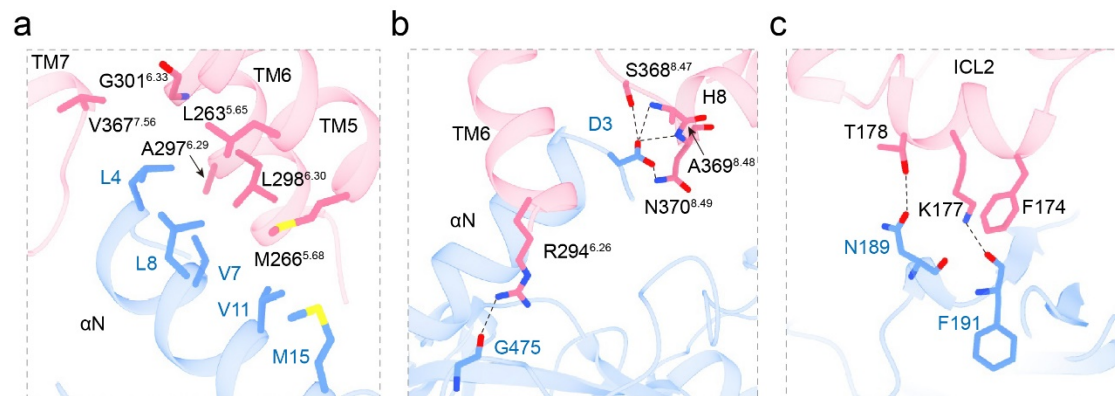
Fig. 3: Interactions between NTSR1 and GRK2. a, b, Detailed interactions at the major interface between the NTSR1 cytoplasmic hydrophobic pocket and GRK2. **c,** Detailed interactions at the minor interface between the ICL2 from NTSR1 and GRK2. NTSR1 is shown in pink and GRK2 is shown in blue.

Figure 4
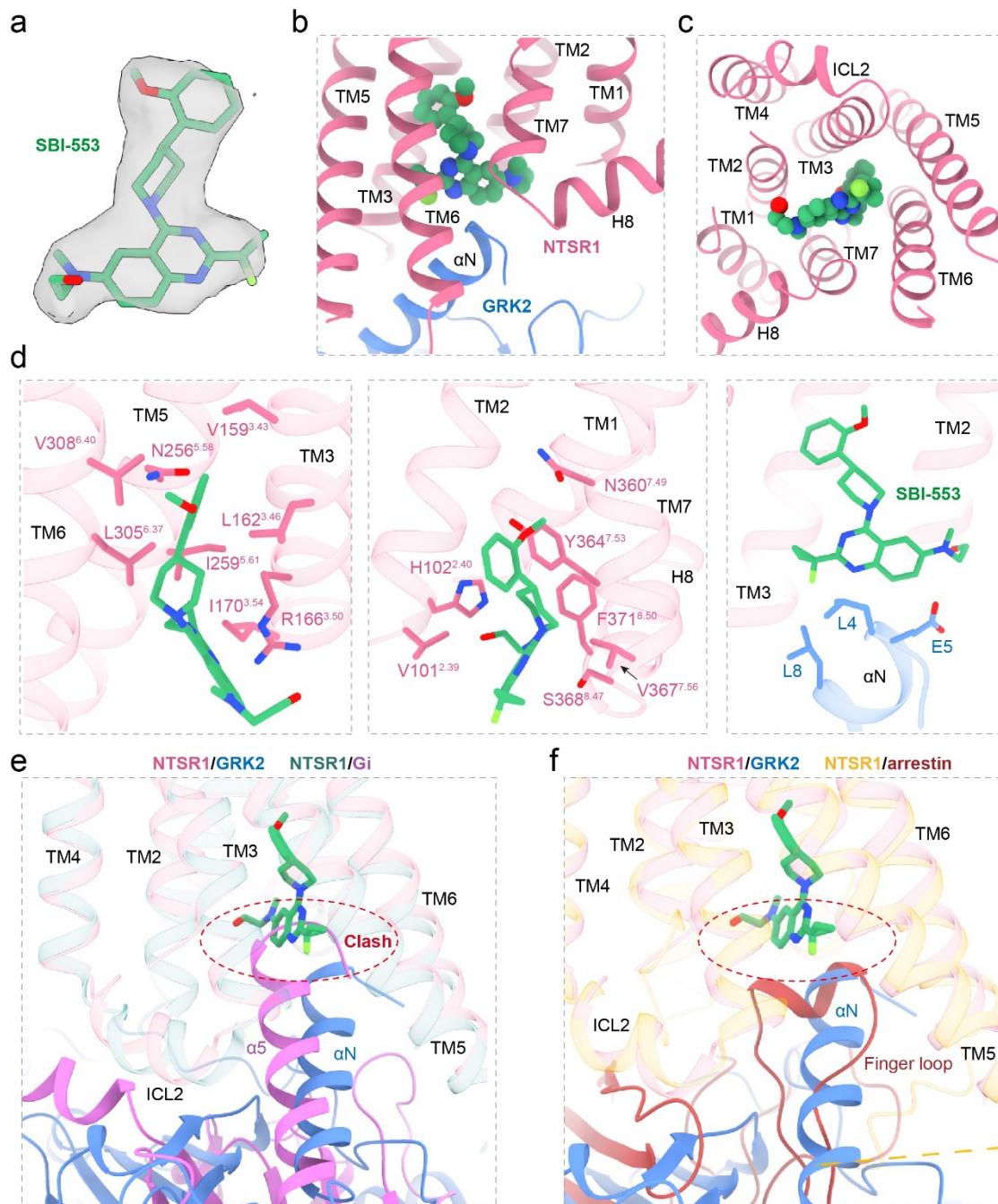
Fig. 4: The binding mode of SBI-553 in NTSR1. a, The EM density of SBI-553, which is shown at a level of 0.12. **b, c,** The binding pocket of SBI-553 in NTSR1, from the front view (**b**) and top view (**c**). SBI-553 is highlighted in sphere. **d**, Detailed interactions between SBI-553 and NTSR1, as well as GRK2. SBI-553 is shown in green, NTSR1 is shown in pink, and GRK2 is shown in blue. **e,** Superposition of the NTSR1 from NTSR1-GRK2-Gαq complex and NTSR1-Gi complex showed the α5 of Gi protein would clash with SBI-553. **f,**

Superposition of the NTSR1 from NTSR1-GRK2-Gαq complex and NTSR1-arrestin complex showed the finger loop of arrestin was compatible with the location of SBI-553.

Figure 5
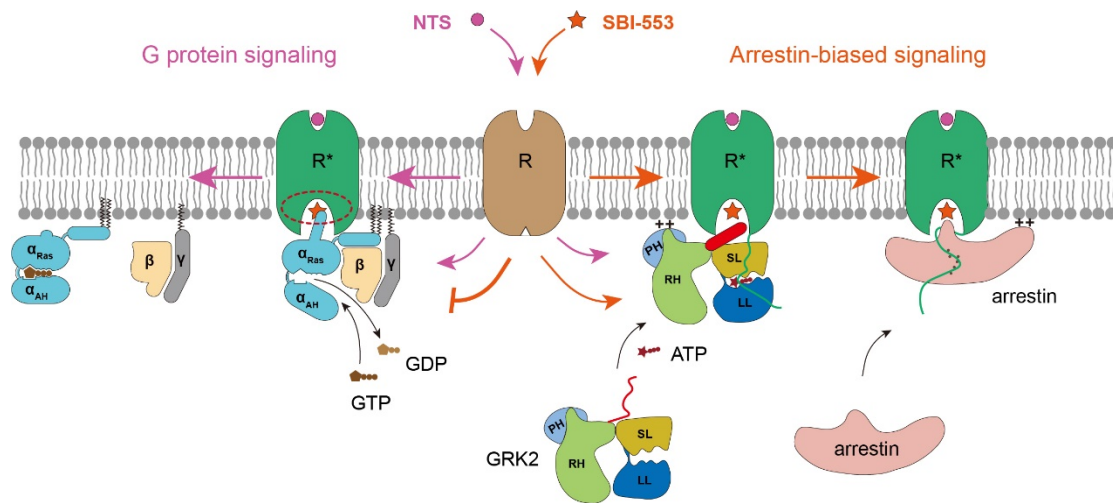
Fig. 5: Cartoon presentation of NTSR1 signaling mediated by G protein and arrestin.
NTS promotes NTSR1 to mediate both G protein and arrestin signaling but SBI-553 blocks
G protein signaling and promotes GRK2 and arrestin signaling. ++ marks indicate
membrane binding.

Extended Data Figure 1
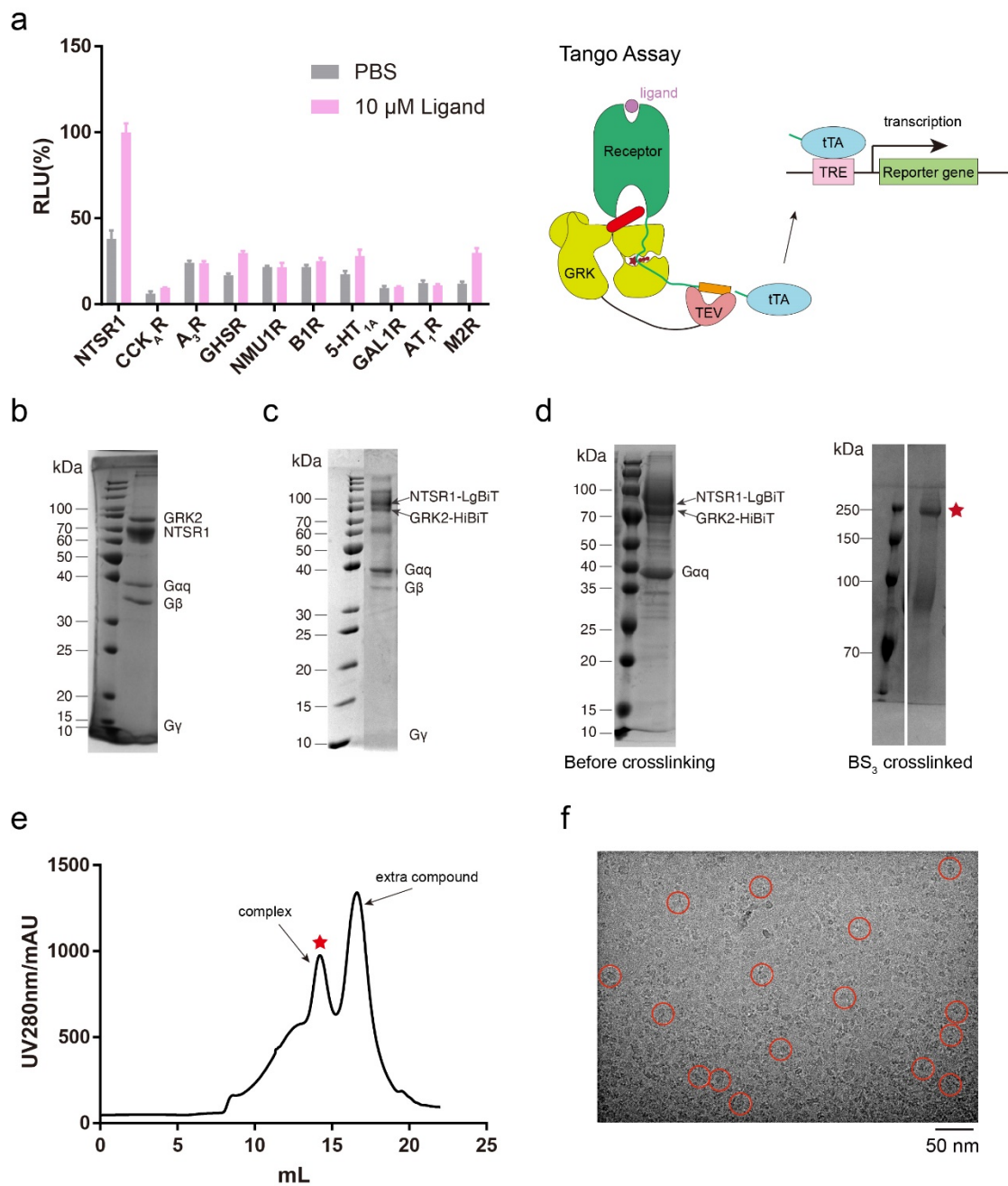
Extended Data Fig. 1 NTSR1-GRK2-Gαq complex assembly. a, Screening for GPCR–GRK2 complexes by tango assay. RLU, relative luciferase units, which was normalized to the values of NTSR1. **b-d** SDS-PAGE of the complexes. NTSR1-GRK2-Gαq-Gβγ complex (**b**), NTSR1_LgBiT-GRK2_HiBiT-Gαq-Gβγ complex (**c**), NTSR1-GRK2-Gαq complex before crosslinking (left panel of **d**) and NTSR1-GRK2-Gαq complex crosslinked by BS$_3$ (right panel of **d**). **e,** Size-exclusion chromatography elution profile of the NTSR1-GRK2-Gαq complex. Red star indicates the monomer peak of the complex. **f,** Cryo-EM

micrograph of the NTSR1-GRK2-Gαq complex. Particles picked for 3D classifications were highlighted in red circles.

Extended Data Figure 2
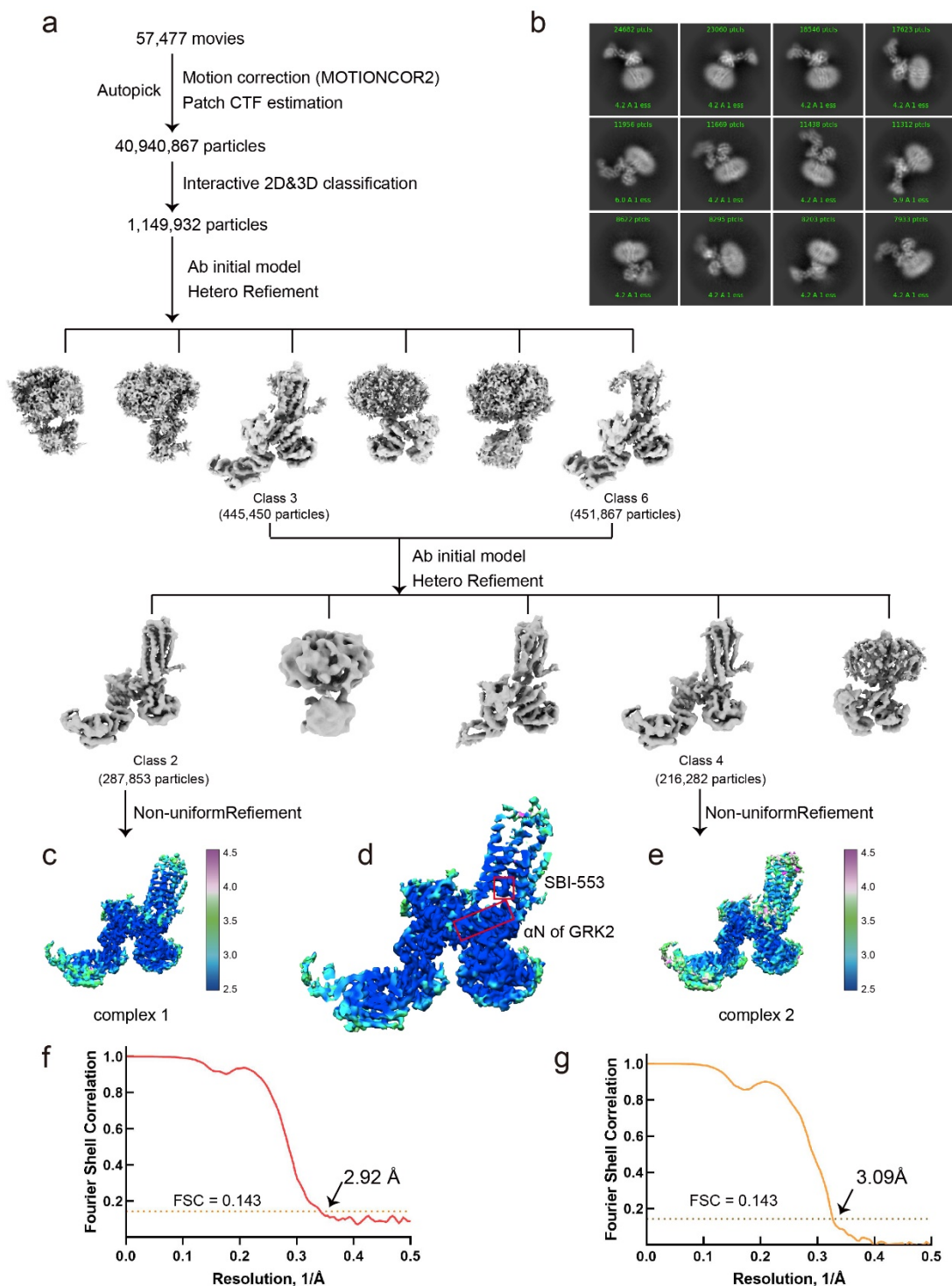
Extended Data Fig. 2 Single-particle reconstruction of the NTSR1-GRK2-Gαq complex. a, Flowchart of cryo-EM data analysis of the NTSR1-GRK2-Gαq complex. **b,** Micrograph of the reference-free 2D class averages. **c-e,** Two cryo-EM maps of the NTSR1-GRK2-Gαq complexes were generated and colored by local resolutions from 2.5

Å (blue) to 4.5 Å (purple) (**c and e**). The first map is enlarged for the clarity of SBI-553 and αN of GRK2. SBI-553 and αN of GRK2 are highlighted in red squares (**d**). **f, g,** The "Gold-standard" Fourier shell correlation (FSC) curve indicates that the overall resolution of the electron density map of the NTSR1-GRK2-Gαq complex 1 is 2.92 Å, the NTSR1-GRK2-Gαq complex 2 is 3.09 Å.

Extended Data Figure 3

TM1   TM2   TM3   TM4   TM5   TM6   TM7

H8   staurosporine   GDP•Mg^{2+}•AlF$_4^-$ αN
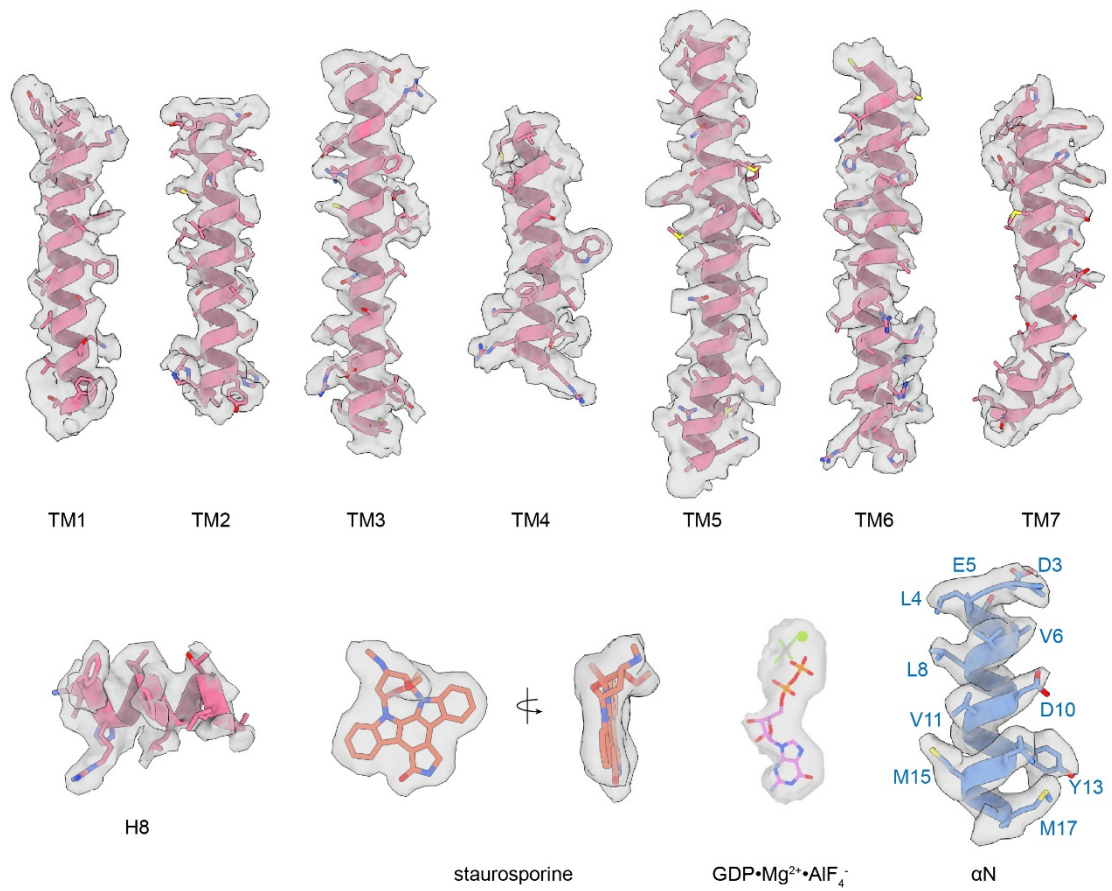
Extended Data Fig. 3 Cryo-EM density maps with all transmembrane helices, and H8 of NTSR1, staurosporine, GDP·Mg^{2+}·AlF$_4^-$ and αN of GRK2.

Extended Data Figure 4
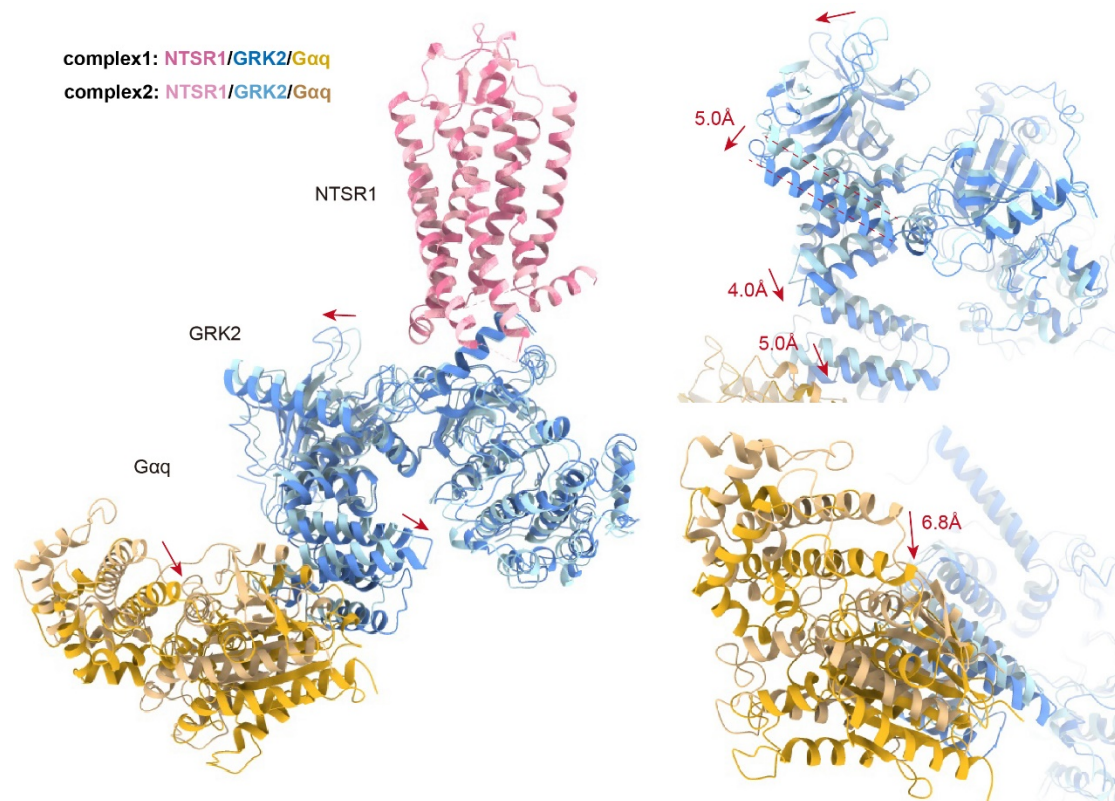
Extended Data Fig. 4 Structural comparison of the NTSR1-GRK2-Gαq complex1 and 2. Comparison of these two complexes reveals that they have very similar NTSR1 structure but a swing of GRK2 and Gαq of ~5-6 Å related to NTSR1.

Extended Data Figure 5
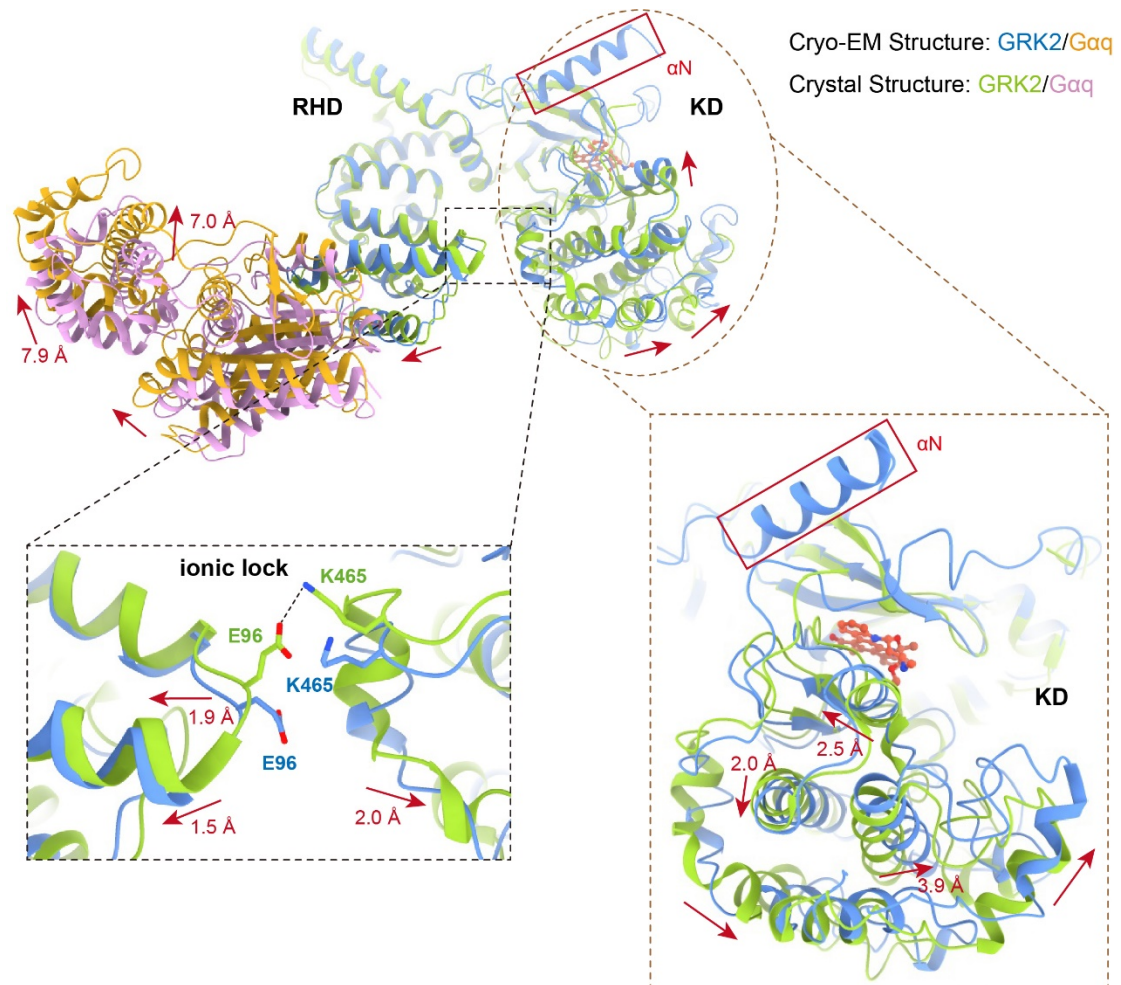
Extended Data Fig. 5 Structural comparison of the GRK2-Gαq from the cryo-EM structure NTSR1-GRK2-Gαq complex with the crystal structure of GRK2-Gαq-Gβγ. Comparing the GRK2 structure from the NTSR1 complex to the crystal structure of GRK2 from the complex with Gαq and Gβγ reveals three major differences. The GRK2 structure from the NTSR1 complex contains a N-terminal helix that is packed onto the kinase domain, has a breakage in the ionic lock between its RHD from the KD, and adopts a closed conformation in its KD by 2-3 Å shifts of the KD relative to the KD of GRK2 from the crystal structure.

Extended Data Figure 6

```
                    18        23        30                              54
GRK2  ---MADLEAVLADVSYLMAME--KSKATPAARASKKILLPEPSIRSVMQKYLEDRGEVTFEKIFSQKLGYLLFRDFCLNHLEEARPLV
GRK3  ---MADLEAVLADVSYLMAME--KSKATPAARASKRIVLPEPSIRSVMQKYLAERNEITFDKIFNQKIGFLLFKDFCLNEINEAVPQV
GRK4  ----MELENIVANSLLLKARQ--GGYGKKSGRSKKWKEILTLPPVSQCSELRHSIEKDYSSLCDKQPIGRRLFRQFCD-TKPTLKRHI
GRK5  ---MELENIVANTVLLKARE--GGGGKRKGKSKKWKEILKFPHISQCEDLRRTIDRDYCSLCDKQPIGRLLFRQFCE-TRPGLECYI
GRK6  ---MELENIVANTVLLKARE--GGGGNRKGKSKKWRQMLKFPHISQCEELRLSLERDYHSLCERQPIGRLLFREFCA-TRPELSRCV
GRK7  MVDMGALDNLIANTAYLQARKPSDCDSKELQRRRRSLA---LPGLQGCAELRQKLSLNFHSLCEQQPIGRRLFRDFLA-TVPTFRKAA
GRK1  -MDFGSLETVVANSAFIAARGSFDGSSSQPSRDKKYLAKLKLPPLSKCESLRDSLSLEFESVCLEQPIGKKLFQQFLQ-SAEKHLPAL
```
    αN   NLBD   RHD   α1   α2   α3   α4

```
GRK2  EFYEEIKKYEKLETEEERVARSREIFDSYIMKELL-ACSHPFSKSATEHVQGHLGKKQVPPDLFQPYIEEICQNLRGDVFQKFIESDK
GRK3  KFYEEIKEYEKLDNEEDRLCRSRQIYDAYIMKELL-SCSHPFSKQAVEHVQSHLSKKQVTSTLFQPYIEEICESLRGDIFQKFMESDK
GRK4  EFLDAVAEYEVADDEDRSDCGLS-ILDRFFNDKLA-APLPEIPPDVVTECRLGLKEENPSKKAFEECTRVAHNYLRGEPFEEYQESSY
GRK5  QFLDSVAEYEVTPDEKLGEKGKE-IMTKYLTPKSP-VFIAQVGQDLVSQTEEKLLQ-KPCKELFSACAQSVHEYLRGEPFHEYLDSMF
GRK6  AFLDGVAEYEVTPDDKRKACGRQ-LTQNFLSHTGP-DLIPEVPRQLVTNCTQRLEQ-GPCKDLFQELTRLTHEYLSVAPFADYLDSIY
GRK7  TFLEDVQNWELAEEGPTKDSALQGLVATCASAPAPGNPQPFLSQAVATKCQAATTE-EERVAAVTLAKAEAMAFLQEQPFKDFVTSAF
GRK1  ELWKDIEDYDTADN-DLQPQKAQTILAQYLDPQAKLFCS-FLDEGIVAKFKEGPVE-IQDGLFQPLLQAT-LAHLGQAPFQEYLGSLY
```
     α4   α5   α6   α7

```
           175              193
GRK2  FTRFCQWKNVELNIHLTMNDFSVHRIIGRGGFGEVYGCRKADTGKMYAMKCLDKKRIKMKQGETLALNERIMLSLVSTGDCPFIVCMS
GRK3  FTRFCQWKNVELNIHLTMNEFSVHRIIGRGGFGEVYGCRKADTGKMYAMKCLDKKRIKMKQGETLALNERIMLSLVSTGDCPFIVCMT
GRK4  FSQFLQWKWLER-QPVTKNTFRHYRVLGKGGFGEVCACQVRATGKMYACKKLQKKRIKKRKGEAMALNEKRILEKVQS---RFVVSLA
GRK5  FDRFLQWKWLER-QPVTKNTFRQYRVLGKGGFGEVCACQVRATGKMYACKRLEKKRIKKRKGESMALNEKQILEKVNS---QFVVNLA
GRK6  FNRFLQWKWLER-QPVTKNTFRQYRVLGKGGFGEVCACQVRATGKMYACKKLEKKRIKKRKGEAMALNEKQILEKVNS---RFVVSLA
GRK7  YDKFLQWKWLFEM-QPVSDKYFTEFRVLGKGGFGEVYGCVKNTGKMYACKKLDKKRLKKKGGEKMALLEKEILEKVSS---PFIVSLA
GRK1  FLRFLQWKWLEA-QPMGEDWFLDFRVLGKGGFGEVSACQMKATGKLYACKKLNKKRLKKRKGYQGAMVEKKILMKVHS---RFIVSLA
```
     α8   β1   β2   β3   β4   α1   α2   KD

```
GRK2  YAFHTPDKLSFILDLMNGGDLHYHLSQHG----VFSEADMRFYAAEIIILGLEHMHNRFVVYRDLKPANILLDEHGHVRISDLGLACDF
GRK3  YAFHTPDKLCFILDLMNGGDLHYHLSQHG----VFSEKEMRFYATEIIILGLEHMHNRFVVYRDLKPANILLDEHGHARISDLGLACDF
GRK4  YAYETKDALCLVLTIMNGGDLKFHIYNLG--NPGFDEQRAVFYAAELCCGLEDLQRERIVYRDLKPENILLDDRGHIRISDLGLATEI
GRK5  YAYETKDALCLVLTIMNGGDLKFHIYNMG--NPGFEEERALFYAAEILCGLEDHRENTVYRDLKPENILLDDYGHIRISDLGLAVKI
GRK6  YAYETKDALCLVTLMNGGDLKFHIYNLG--QAGFPEARAVFYAAEICCGLEDLHRERIVYRDLKPENILLDDHGHIRISDLGLAVHV
GRK7  YAFESKTHLCLVMSLMNGGDLKFHIYNVG--TRGLDMSRVIFYSAQIACGMLHLHELGIVYRDMKPENVLLDDLGNCRLSDLGLAVEM
GRK1  YAFETKADLCLVMTIMNGGDIRYHIYNVNEENPGFPEPRALFYTAQIICGLEHLHQRRIVYRDLKPENVLLDNDGNVRISDLGLAVEL
```
   β5   β6   α3   α4   β7   β8

```
GRK2  SKKK--PHASVGTHGYMAPEVLQKGVAYDSSADWFSLGCMLFKLLRGHSPFRQHKTKDK-HEIDRMTLTMAVELP-DSFSPELRSLLE
GRK3  SKKK--PHASVGTHGYMAPEVLQKGTAYDSSADWFSLGCMLFKLLRGHSPFRQHKTKDK-HEIDRMTLTVNVELP-DTFSPELKSLLE
GRK4  PEGQ-RVRGRVGTVGYMAPEVVNNEK-YTFSPDWWGLGCLIYEMIQGHSPFKKYKEKVKWEEVDQRIKNDTEEYS-EKFSEDAKSICR
GRK5  PEGD-LIRGRVGTVGYMAPEVLNNQR-YGLSPDYWGLGCLIYEMIEGQSPFRGRKEKVKREEVDRRVLETEEVYS-HKFSEEAKSICK
GRK6  PEGQ-TIKGRVGTVGYMAPEVVKNER-YTFSPDWWALGCLLYEMIAGQSPFQQRKKIKREEVERLVKEVPEEYS-ERFSPQARSLCS
GRK7  KGGKPITQ-RAGTNGYMAPEILMEKVSYSYPVDWFAMGCSIYEMVAGRTPFKDYKEKVSKEDLKQRTLQDEVKFQHDNFTEEAKDICR
GRK1  LDGQSKTKGYAGTPGFMAPELLQGEE-YDFSVDYFALGVTLYEMIAARGPFRARGEKVENKELKHRIISEPVKYP-DKFSQASKDFCE
```
     α5   α6   α7

```
                                        475
GRK2  GLLQRDVNRRLGCLGRGAQEVKESPFFRSLDWQMVFLQKYPPPLIPPRGEVNAADAFDIGSFDEEDTKGIKLLDSDQELYRNFPL-TI
GRK3  GLLQRDVSKRLGCHGGGSQEVKEHSFFKGVDWQHVYLQKYPPPLIPPRGEVNAADAFDIGSFDEEDTKGIKLLDCDQELYKNFPL-VI
GRK4  MLLTKNPSKRLGCRGEGAAGVKQHPVFKDINFRRLEANMLEPPFCPDPHAVYCKDVLDIEQFS--VVKGIYLDTADEDFYARFATGCV
GRK5  MLLTKDAKQRLGCQEEGAAKVKRHPFFRNMNFKRLEAGMLDPPFVPDPRAVYCKDVLDIEQFS--TVKGVNLDHTDDDFYSKFSTGSV
GRK6  QLLCKDPAERLGCRGGGSAREVKEHPLFKKLNFKRLGAGMLEPPFKPDPQAIYCKDVLDIEQFS--TVKGVELEPTDQDFYQKFATGSV
GRK7  LFLAKKPEQRLGSR-EKSDDPRKHHFFKTINFPRLEAGLIEPPFVPDPSVVYAKDIAEIDDFS--EVRGVEFDDKDKQFFKNFATGAV
GRK1  ALLEKDPEKRLGFRDETCDKLRAHPLFKDLNWRQLEAGMLMPPFIPDSKTVYAKDIQDVGAFS--TVKGVAFDKTDTEFFQEFATGNC
```
   α7   α8   α9   AST

```
                                   553    558          572
GRK2  SERWQQEVAET-VFDTINAETDRLEARKKAKNKQLGHEEDYALGKDCIMHGYMSKMGNPFLTQWQRRYFYLFPNRLEWRGEGEAPQSL
GRK3  SERWQQEVTET-VYEAVNADTDKIEARKRAKNKQLGHEEDYALGKDCIMHGYMLKLGNPFLTQWQRRYFYLFPNRLEWRGEGESRQNL
GRK4  SIPWQNEMIESGCFKDINKSESEEALPLDLDKNIHTPVSRPNRGFFYRLFRRGG--CLTMVPSEKEVEPKQC----------------
GRK5  SIPWQNEMIETECFKELNVFGPNGTLPPDLNRN-HPPEP-PKKGLLQRLFKRQHQNNSKSSPSSKTSFNHHINSNHVSSNSTGSS---
GRK6  PIPWQNEMVETECFQELNVFGLDGSVPPDLDWKGQPPAP-PKKGLLQRLFSRQD--CCGNCSDSEEELPTRL----------------
GRK7  PIAWQEEIIETGLFEELN----D---PNRPTGCEEGNS--SKSGVCLLL-----------------------------------------
GRK1  PIPWQEEMIETGIFGELNVWRSDGQMPDDMKGISGGSSSSKSGMCLVS-----------------------------------------
```
     α9   CLBD   β1   PHD   β2   β3   β4

```
           614
GRK2  LTMEEIQSVEETQIKERKCLLLKIRGGKQFILQCDSDPELVQWKKELRDAYREAQQLVQRVPKMKNKPRSPVVELSKVPLVQRGSANG
GRK3  LTMEQILSVEETQIKDKKCILFRIKGGKQFVLQCESDPEFVQWKKELNETFKEAQRLLRRAPKFLNKPRSGTVELPKPSLCHR-NSNG
```
    β5   β6   α helix

Extended Data Fig. 6 Sequence alignment of human GRKs. The N-terminal helix (αN) is highlighted in red. The RHD is highlighted in green and KD is in light blue. The AST loop

extended from the kinase domain is in light purple. The PHD of GRK2 and GRK3 are in pink. N-terminal lipid binding domain (NLBD) and C-terminal lipid binding domain (NLBD) according to GRK5 are highlighted in dark yellow and light green, respectively. Residues that may interact with membrane lipid are highlighted in dark blue. And residues from GRK2 that interact with NTSR1 are highlighted in yellow. α, α helix. β, β strand.
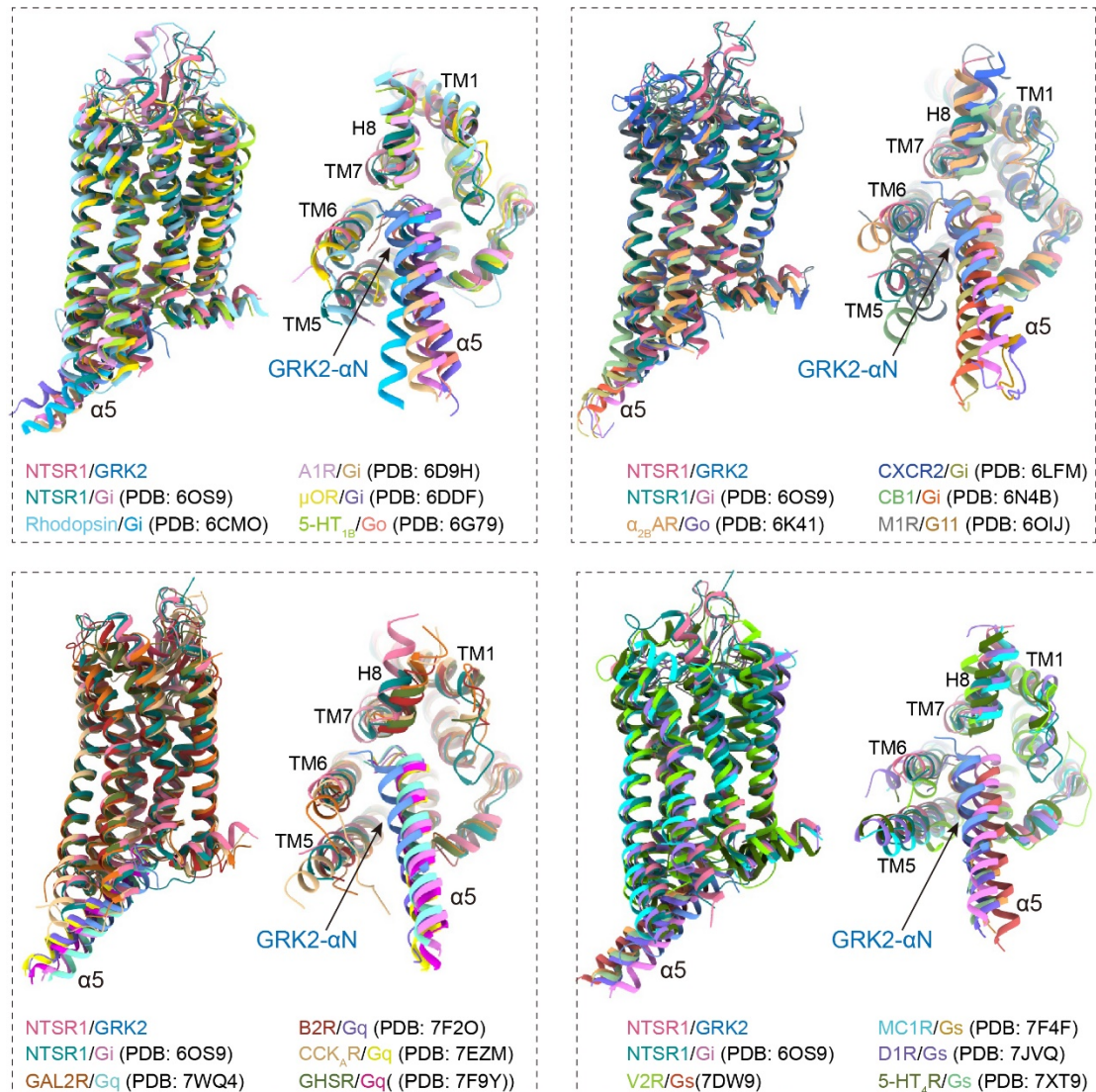
Extended Data Figure 7
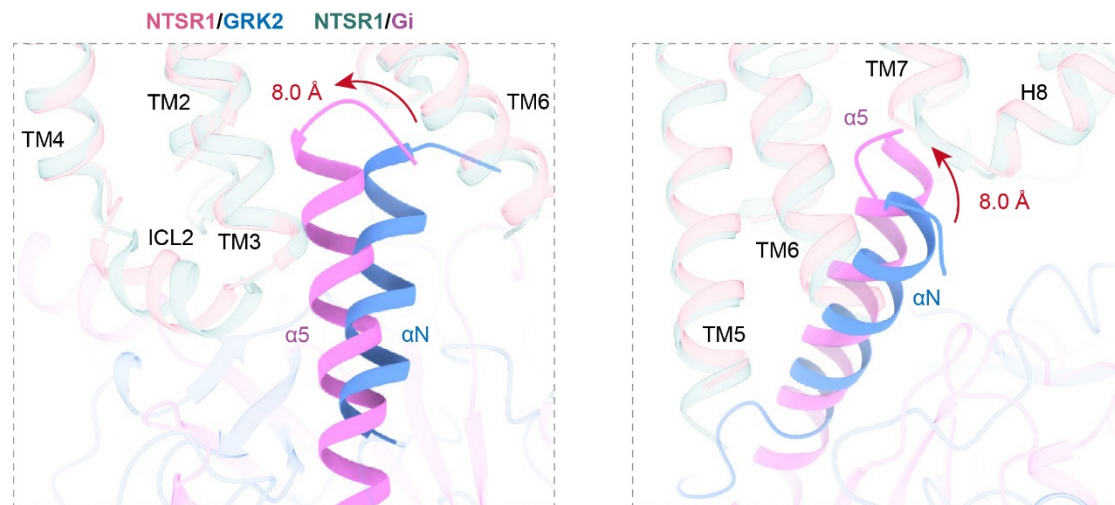
Extended Data Fig. 7 Structural comparison of NTSR1-GRK2-Gαq complex with NTSR-Gi complex. Superposition of the NTSR1 from NTSR1-GRK2-Gαq complex and NTSR1-Gi complex showed the α5 helix from the Gαi is up-shift by 8.0 Å into the TMD pocket related to the N-terminal helix of GRK2.

Extended Data Figure 8

Extended Data Fig. 8 Structural comparison of NTSR1-GRK2-Gαq complex with NTSR-Gi complex and other GPCR-G protein complexes. Superposition of the receptors from different GPCR complexes showed that the active GPCRs had very similar 3D architecture, and the location of α5 helix from different G proteins overlapped with the N-terminal helix of GRK2.

Extended Data Table 1 Cryo-EM data collection, refinement and validation statistics.

	NTSR1-GRK2-Gαq complex1 (EMDB-xxxx) (PDB xxxx)	NTSR1-GRK2-Gαq complex2 (EMDB-xxxx) (PDB xxxx)
Data collection and processing		
Magnification	57,477	
Voltage (kV)	300	
Electron exposure (e–/Å^2)	50	
Defocus range (μm)	-1.2 to -2.2	
Pixel size (Å)	0.824	
Symmetry imposed	C1	
Initial particle images (no.)	40,940,867	
Final particle images (no.)	287,853	216,282
Map resolution (Å)	2.92	3.09
FSC threshold	0.143	0.143
Map resolution range (Å)	2.5 – 4.5	2.5 – 4.5
Refinement		
Initial model used (PDB code)	2BCJ, AlphaFold-NTSR1	2BCJ, AlphaFold-NTSR1
Map sharpening B factor (Å^2)	-103.4	-90.9
Model composition		
Non-hydrogen atoms	10575	10575
Protein residues	1290	1290
Ligands	4	4
Nucleotide	1	1
B factors (Å^2)		
Protein	80.06	80.06
Ligand	47.08	47.08
Nucleotide	76.30	76.30
R.m.s. deviations		
Bond lengths (Å)	0.005	0.005
Bond angles (°)	0.989	0.989
Validation		
MolProbity score	1.77	1.83
Clashscore	4.23	4.94
Poor rotamers (%)	0.00	0.00
Ramachandran plot		
Favored (%)	94.99	95.07
Allowed (%)	5.01	4.93
Disallowed (%)	0.00	0.00

Extended Data Table 2 Interactions of SBI-553 with NTSR1 and GRK2

	V101$^{2.39}$	NTSR1
	H102$^{2.40}$	
	V159$^{3.43}$	
	L162$^{3.46}$	
	R166$^{3.50}$	
	I170$^{3.54}$	
	N256$^{5.58}$	
	I259$^{5.61}$	
SBI-553	L305$^{6.37}$	
	V308$^{6.40}$	
	N360$^{7.49}$	
	Y364$^{7.53}$	
	V367$^{7.56}$	
	S368$^{8.47}$	
	F371$^{8.50}$	
	L4	GRK2
	E5	
	L8	

Supplementary Files

This is a list of supplementary files associated with this preprint. Click to download.

- ExtendedDataMovie.mp4